

A geometrically informed algebraic multigrid preconditioned iterative approach for solving high-order finite element systems

Songzhe Xu^{a,d}, Majid Rasouli^b, Robert M. Kirby^{a,b}, David Moxey^c, Hari Sundar^{b,*}

^a*Scientific Computing and Imaging Institute, University of Utah, USA*

^b*School of Computing, University of Utah, USA*

^c*College of Engineering, Mathematical and Physical Sciences, University of Exeter, UK*

^d*State Key Laboratory of Advanced Special Steels, School of Materials Science and Engineering, Shanghai University, Shanghai, China*

Abstract

Algebraic multigrid (AMG) is conventionally applied in a black-box fashion, agnostic to the underlying geometry. In this work, we propose that using geometric information – when available – to assist with setting up the AMG hierarchy is beneficial, especially for solving linear systems resulting from high-order finite element discretizations. High-order problems draw considerable interest to both the scientific and engineering communities, but lack efficient solvers, at least open-source codes, tailored for unstructured high-order discretizations targeting large-scale, real-world applications. For geometric multigrid, it is known that using p -coarsening before h -coarsening can provide better scalability, but setting up p -coarsening is non-trivial in AMG. We develop a geometrically informed algebraic multigrid (GIAMG) method, as well as an associated high-performance computing program, which is able to set up a grid hierarchy that includes p -coarsening at the top grids with minimal information of the geometry from the user. A major advantage of using p -coarsening with AMG – beyond the benefits known in the context of geometric multigrid (GMG) – is the increased sparsification of coarse grid operators. We extensively evaluate GIAMG by testing on the 3D Helmholtz and incompressible flow problems, and demonstrate mesh-independent convergence, and excellent parallel scalability. We also compare the performance of GIAMG with existing AMG packages, including Hypre and ML.

Keywords: high-order or spectral/ hp element; geometrically informed algebraic multigrid; p -coarsening; preconditioning; high-performance computing

Contents

1	Introduction	2
----------	---------------------	----------

*Corresponding author

Email address: hari@cs.utah.edu (Hari Sundar)

2 Algorithms and implementations	6
2.1 Required geometric information	7
2.2 Computation of $l2g$ map at each level	8
2.3 Parallel implementation	9
2.4 Forming prolongation	10
2.5 h-coarsening	11
3 Experiments and results	11
3.1 Helmholtz operator	11
3.1.1 Convergence results	12
3.1.2 Comparison with other solvers at $p = 8$	12
3.2 Incompressible flow problem	14
3.2.1 Convergence results	15
3.2.2 Detailed analysis at $p = 5$	15
4 Conclusions and future work	20

1. Introduction

The development of robust, efficient solvers that utilize high-order finite element methods (HO-FEM), also sometimes classified as spectral/ hp element methods, is an area of considerable interest to both the scientific and engineering communities [1, 2]. The use of higher order polynomial expansions within elements carries a number of benefits, as seen from two main perspectives. Numerically, these methods exhibit far lower levels of numerical dispersion and dissipation at higher polynomial orders, which makes them a particularly well-suited approximation choice in areas such as computational fluid dynamics (CFD). CFD generally solves governing equations involving Navier–Stokes equations, or their variations, to study the fluid-related physics. Among the traditional methods for numerically solving fluid mechanics, finite volume method is the most popular approach due to its better performance for the conservation laws, while finite element method rapidly develops in recent decades as approaches (such as Petrov-Galerkin [3], discontinuous Galerkin [4], velocity correction [5], etc) have been proposed to successfully address the non-symmetric convection term. In CFD, the trend of increasing computational power has led to interest in large-eddy simulation (LES) or direct numerical simulation (DNS) at increasing levels of fidelity [6]. In this context, the accurate advection of energetic vortices and other fluid structures over large time- and length-scales is a key concern, for example in the simulation of jetting vortices [7], and these numerical properties help to preserve and accurately represent such structures on relatively coarse grids that would be otherwise very diffusive at lower orders. This enables a

more effective balance to be achieved between accuracy and computational efficiency, whilst the elemental decomposition of the method permits complex geometries such as whole car simulations to be considered [8]. Furthermore, given current hardware trends, another appealing property of these methods has been their computational performance. Although the cost per degree of freedom in terms of algorithmic floating point operations (FLOPS) increases substantially with polynomial degree, the use of higher order expansions leads to formulations of the underlying equations of state that involve dense, compact kernels for key finite element operators, such as inner products and derivatives. This is important from the perspective of modern hardware, where increasingly the bottleneck in performance is memory bandwidth as opposed to the clock speed of processors. The underlying arithmetic intensity of the algorithm at hand (i.e., the number of floating-point operations performed for each memory operation) is therefore key to attaining optimal performance. This is where high-order methods have a significant advantage over lower order methods (e.g., [9, 10]).

The main challenges in high-order discretizations are that matrices are more dense compared with low-order methods, and that they lose structural properties such as the M–matrix property, which often allows one to prove convergence of iterative solvers. For our target applications, multigrid is a preferred method for solving the resulting symmetric linear systems with optimal and mesh-independent convergence [11]. However, when used with unstructured meshes, the use of geometric multigrid (GMG) is not straightforward, requiring the use of algebraic multigrid (AMG) instead. Unlike GMG, where the coarse-grid operators are typically obtained via geometric coarsening and rediscretizations, AMG does not use the geometric information but instead builds the coarse grid operators algebraically. Algebraic coarsening results in a loss of sparsity, leading to poor performance and scalability, especially for large-scale problems. This is usually addressed by employing sparsity control techniques, such as dropping values below a specified threshold at coarser levels. Such measures can address the sparsity issues, albeit with some loss of convergence rates. Additionally, they introduce an additional parameter that needs to be tuned, making the overall solver or preconditioner less robust. This issue is exacerbated for high-order operators that are denser to begin with, and get even denser on coarser grids, leading to poor scalability.

There are two major possibilities for constructing a multigrid hierarchy for high-order discretizations: (1) algebraical h -coarsening, in which the mesh is coarsened based on the specific matrix properties; and (2) p -coarsening, in which the problem is coarsened by reducing the polynomial order of the basis functions and degrees of freedom within each element, resulting in a local coarsening. While using the geometric information within AMG is not really that beneficial for traditional h -coarsening (both problems are equivalent to graph coarsening), p -coarsening can be applied in an element-local fashion, and importantly helps sparsify the operator before traditional AMG coarsening is applied. The overall coarsening strategy is illustrated in Figure 1. In this work,

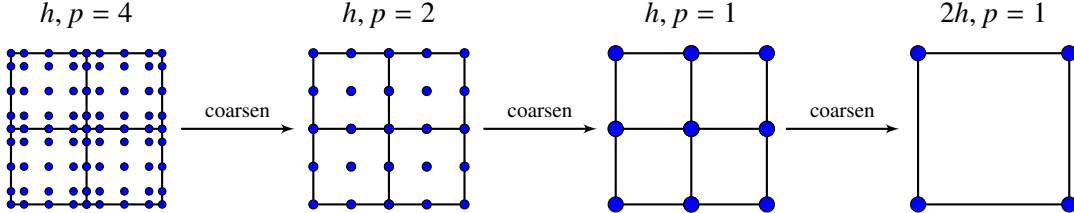


Figure 1: Illustration of the coarsening strategy of GIAMG for quadrilateral elements with nodal basis of polynomial order $p = 4$. First, we p -coarsen from $p = 4$ to $p = 2$, and then again p -coarsen from $p = 2$ to $p = 1$. The total number of elements—and therefore the mesh—does not change during p -coarsening. Once we reach linear elements, we perform h -coarsening to obtain a coarser mesh and smaller system.

we thoroughly evaluate this concept and demonstrate its efficacy in handling complex operators on complex geometries.

For the grids obtained using p -coarsening, we effectively increase the sparsity as we go to coarser levels. This enables us to offset the loss of sparsity encountered when generating coarser levels using AMG. This plays a major part in ensuring that the overall scalability remains good. In addition, if the high-order system is generated using a nodal basis, it interpolates the prolongation matrix values using lower order basis at higher order nodes. If using a modal basis, then the restriction operation is simply an “injection”, i.e., a lower order mode is injected to the coarser level. This indicates the prolongation and restriction operators will only have zero- or unity-valued entries, and the sparsity of coarser level matrices is further reduced compared to using a nodal basis. As a result, it is extremely efficient to perform p -coarsening for such high-order systems.

Related work: Multigrid for high-order or spectral/ hp elements has been studied as early as in the 1980s. The use of p -coarsening is rather common in the context of high-order discontinuous Galerkin discretizations [12, 13], but it has also been used for continuous finite element discretizations [14, 15] and mixed finite element method [16]. A popular strategy for high-order discretizations on unstructured meshes, for which p -coarsening is challenging, is to assemble a low-order approximation of the high-order system and use an algebraic multigrid method to invert the low-order (and thus much sparser) operator [17–21]. In [22], this approach is compared with the direct application of algebraic multigrid to the high-order operator, and the authors find that one of the main difficulties is the assembly of the low-order approximation required by algebraic multigrid methods. To the best of our knowledge, prior works have not considered using geometric information to assist in setting up the grid hierarchy.

Contributions: While several approaches have been proposed to solve high-order systems using geometric multigrid, or reducing the operator to design AMG-based preconditioners, there has been limited work on applying AMG directly to the high-order systems. In addition, there is a distinct lack of scalable, open-source solvers for unstructured high-order discretizations targeting large-scale, real-world applications. In this paper, we proposed a geometrically informed algebraic

multigrid (GIAMG) for solving high-order finite element systems in engineering applications, especially for the systems resulting from fluid mechanics as our target application. In a broad sense, the GIAMG method would work for physics problems that can be cast to symmetric systems (operators such as Poisson, Helmholtz, etc), depending on the properties of matrices. We also developed a high-performance computing code making use of open-source finite element and AMG libraries. This GIAMG solver employs a p -coarsening strategy with assistance of minimal provided geometric information followed by an AMG h -coarsening after the order of basis functions that form the original high-order systems is reduced to linear (or some low order). We perform comprehensive experiments and comparisons with other multigrid methods to demonstrate the performance of this GIAMG solver.

While this work is motivated by developing a scalable parallel solver for high-order finite element systems, all the matrices used in the experiments are formed from a well-recognized open-source spectral/ hp element library – *Nektar++* [23, 24]. This work is also based on our previously developed smoothed-aggregate AMG (SAAMG) library – *Saena* [25] for the h -coarsening in the GIAMG approach. The code for the GIAMG solver is available on https://github.com/paralab/saena_giamg under the MIT license. While we have used the open-source *Nektar++* and *Saena* libraries, the GIAMG code can easily be modified to use other high-order finite-element packages such as *deal.II* [26], *MOOSE* [27] and *MFEM* [28], and AMG packages such as *ML* [29] and *Hypre* [30].

Limitations: Limited geometric information, which is available in *Nektar++* as well as most high-order finite element packages, currently needs to be passed to the GIAMG solver. Note, the GIAMG solver is not limited to be used with *Nektar++*, we only use *Nektar++* as an example demonstration in this work. The GIAMG solver has an interface to take necessary geometric information passed from high-order finite element packages and convert the information to its own data structure. The information needed is limited to identifying which degrees-of-freedom (dof) can be grouped together as an element, as well as their role within the elemental basis. This makes GIAMG solver not a pure AMG solver (as a result, so-called geometrically informed). It is challenging to automatically identify such information purely from the input matrices, which is the bottle-neck to make GIAMG a complete *black-box* AMG solver for solving high-order finite element systems. We are currently working on efficient methods to identify this information directly from the discretized operators. In addition, the GIAMG solver currently only works with symmetric systems for optimal convergence, and therefore treatment is required for non-symmetric terms in Navier–Stokes equations (e.g., using the velocity correction scheme).

The rest of the paper is organized as follows. In § 2, we describe in detail the algorithms and implementation of GIAMG method used for high-order systems. In § 3, we present comprehensive experiments and comparisons with other available multigrid packages using 3D test problems.

Finally, in § 4 we draw conclusions and discuss future research directions.

2. Algorithms and implementations

Consider a linear system

$$Ax = b \quad (1)$$

where A is a linear operator, b is a right-hand-side vector, and x is the solution vector. The multigrid v-cycle is the standard building block for both multigrid as a solver, as well as when used as a preconditioner with the conjugate gradient method. We therefore start by summarizing the overall process of applying a v-cycle of the proposed GIAMG method. The v-cycle algorithm is presented in Algorithm 1.

Algorithm 1 GIAMG process

```

1: procedure V-CYCLE
2:   if coarsest level then
3:     Directly solve the coarsest matrix
4:     return
5:   end if
6:   Presmooth
7:   Compute residual
8:   if  $p$ -coarsening level then
9:      $p$ -restrict residual
10:   else
11:      $h$ -restrict residual
12:   end if
13:   V-CYCLE
14:   if  $p$ -coarsening level then
15:      $p$ -interpolate error
16:   else
17:      $h$ -interpolate error
18:   end if
19:   Correct solution
20:   PostsMOOTH
21: end procedure

```

At each level, we employ a Jacobi-accelerated Chebyshev smoother for presmoothing. Prolongation and restriction operators are formed according to whether the current grid employs p -coarsening or SAAMG coarsening. The coarser level operator is computed using a Galerkin projection as $A_c = RA_f P$, where A_f is the finer level operator, P and R are prolongation and restriction,

respectively, and $P = R^T$. Note that the coarse-grid operator, as well as the prolongation and restriction operators at each level are precomputed and stored during the setup phase. The finer level residual vector is computed after smoothing as $r_f = b_f - A_f x_f$, where b_f is the finer level right-hand-side and x_f is the current estimate of the finer level solution vector, and restricted to the next coarser level as $r_c = Rr_f$, where r_c is coarser level right-hand-side. A coarser level linear system (error equation) is formed as $A_c e_c = r_c$, where e_c is the coarse-level error vector. This process is recursively repeated until the coarsest level, where we employ a direct solver (superLU [31]) to solve the coarsest system. The coarse-level error vector is then prolonged to be the finer level error vector as $e_f = Pe_c$, and the finer level solution vector is corrected as $x_f = x_f + e_f$. A postsmothing (similar as presmothing) is applied to the corrected solution vector at each level. This process is again recursively repeated until it reaches the finest level to obtain the final solution. The GIAMG approach is used as a preconditioner in this work since the multigrid method is more robust when used as a preconditioner in conjunction with CG [32]. Since we are dealing with symmetric high-order systems, a GIAMG preconditioned conjugate gradient (PCG) iterative solver is employed. One v-cycle of GIAMG is called during the preconditioning, and the rest is the same as standard PCG method. Note during the p -coarsening, we have the flexibility to choose how aggressive, i.e., how many orders of basis to reduce at each level, which can affect the overall convergence (with the SAAMG coarsening levels fixed). We will demonstrate the convergence performance of different p -coarsening strategies in § 3.2. In addition, the computationally dominant part of the GIAMG method is the pre- and postsmothing during the v-cycle. Thus, the performance of the Chebyshev smoother is important, and we want as few iterations (per v-cycle) as possible while still achieving good smoothing at each level. We also demonstrate the effect of smoothing on the overall convergence and total solve time in § 3.2.

One challenge with the GIAMG approach is that additional geometric information, which should be provided by the finite element assembly library, is required at the finest level and needs to be reconstructed at coarser levels to inform how to pick dofs that remain at coarser levels during p -coarsening. This information can be discarded after all the coarse grids are constructed. Note, ideally, it would be optimal to automatically identify such information purely from the matrices. However, it is not easy to extract this information in an efficient and scalable fashion.

2.1. Required geometric information

Since we reduce the basis order within each element, we need to know the elemental dof collection for each element, and also the ordering of the elemental dofs, which implies the basis order at each dof so that we know how to select the dofs that are retained at the next coarser level during p -coarsening. In this work, we use *Nektar++* to assemble the high-order system, and an example of how *Nektar++* orders elemental dofs based on its basis definition is described in the

Appendix. In GIAMG solver, it defines an $l2g$ map, which is the local to global mapping. It is a 2D vector in which a row represents each element, and a column represents collection of elemental dofs. The value of each entry in the $l2g$ map is the dof index in the process matrix. The ordering of entry values in each column (i.e., the ordering of the elemental dofs) in this map implies the basis orders. This procedure is completely parallel, and can be performed independently on each process without any communication. In GIAMG solver, it has an application program interface (API) to take the local to global map from high-order finite element libraries and convert the map to its own $l2g$ map data structure, which requires minimal modification specific to the finite element library data structure. In the parallel case ¹, GIAMG solver defines a $g2u$ map from process dofs to universal system indices. The $g2u$ map is a 1D array with the indices representing dof indices in each process (values of $l2g$ map) and values representing the dof indices in the universal system. GIAMG solver also has an API to convert the data structure of this global to universal map. The local to global and global to universal maps, which are generally available in most of high-order finite element libraries, are the only external arguments that are required in the GIAMG solver.

2.2. Computation of $l2g$ map at each level

For a *Nektar++* hexahedron element type, to extract the dofs that remain to the next coarser level, for example, if we perform a $p \rightarrow p/2$ coarsening (assuming p is an even number), and denote the finer level and coarser level elemental dof collections in each element as df_{arr} and dc_{arr} , respectively, we have Algorithm 2. For other element types, we similarly follow the elemental dof

Algorithm 2 Extract elemental dofs for next level

```

1: procedure EXTRACT_NEXT_DOF( $df_{arr}$ )
2:   for  $i = 0 : p/2$  do
3:     for  $j = 0 : p/2$  do
4:       for  $k = 0 : p/2$  do
5:         Append  $df_{arr}((p + 1)^2 \times i + (p + 1) \times j + k)$  to  $dc_{arr}$ 
6:       end for
7:     end for
8:   end for
9:   return  $dc_{arr}$ 
10: end procedure

```

ordering implied by the definition of basis in those elements (similar as in the Appendix). However, triangular-shaped (including prism) elements have more complicated orderings.

¹In the parallel case, we use “local to global” to represent elemental to process mapping, and “global to universal” to represent process to universal mapping.

With the $l2g$ map and extraction of dofs in the next level, we can first collect all dofs that remain at the next level in an array, denoted as $collect$, by looping over the rows of the $l2g$ map (i.e., looping over elements), as illustrated in Algorithm 3. The indices of the $collect$ will be the

Algorithm 3 Collect all dofs in next level

```

1: procedure DOF_NEXT( $l2g$ ) ▷
2:   for  $e_i = 1 : \text{size}(l2g, 1)$  do
3:      $dc_{arr} = \text{EXTRACT\_NEXT\_DOF}(l2g(e_i, :))$ 
4:     for  $dof = 1 : \text{length}(dc_{arr})$  do
5:       if  $dc_{arr}(dof) \in collect$  then
6:         Skip
7:       else
8:         Append to  $collect$ 
9:       end if
10:      end for
11:    end for
12:    Sort  $collect$ 
13:    return  $collect$ 
14: end procedure

```

values of the next level local to global map, denoted as $l2g_{next}$. Then we build a Hash map, denoted as $hash_{l2g}$, mapping from the $collect$ values (representing finer level $l2g$ values) to its indices (representing coarser level $l2g_{next}$ values). Note, since we perform a sort for $collect$, the coarser level system will have a totally different permutation, which is computed during the sort, compared with the finer level. However, this does not matter since even though we change the permutation in the coarser levels during residual restriction, when we prolong the error back to finer levels, it will be projected back to the original permutation at each level. The $l2g_{next}$ can be then computed as in Algorithm 4. The computation of $l2g_{next}$ will need to be performed at each level. Note, since p -coarsening only reduce p order within elements, the total number of elements remains the same in each level, i.e., the total number of rows is the same in $l2g$ and $l2g_{next}$. Also, in the computation of $l2g_{next}$, boundary nodes need to be carefully handled.

2.3. Parallel implementation

In addition to the $l2g$ map, we need another $g2u$ map for parallel computing. In essence, we have three numberings, the local or elemental numbering, the global or process-local numbering and the universal or the numbering across all dofs on all processes. The $g2u$ map is also read in at the finest level, and we need to re-compute it at each coarser level. We first collect coarser level dofs in each process, and synchronize between all processes to obtain $collect_{univ}$, as shown in Algorithm 5. We then construct a Hash map, $hash_{g2u}$, mapping from $collect_{univ}$'s values to its indices, similarly as $hash_{l2g}$. Now we are able to construct the next coarser level $g2u$ map, $g2u_{next}$,

Algorithm 4 Compute $l2g_{next}$ map in the next level

```

1: procedure L2G_NEXT( $l2g$ )
2:   for  $e_i = 1 : \text{size}(l2g, 1)$  do
3:      $dc_{arr} = \text{EXTRACT\_NEXT\_DOF}(l2g(e_i, :))$ 
4:     for  $dof = 1 : \text{length}(dc_{arr})$  do
5:        $l2g_{next}(e_i, dof) = \text{hash}_{l2g}(dc_{arr}(dof))$ 
6:     end for
7:   end for
8: end procedure

```

Algorithm 5 Obtain universal $collect_{univ}$

```

1: procedure DOF_NEXT_UNIV( $l2g$ )
2:    $collect = \text{DOF\_NEXT}(l2g)$ 
3:   Gather  $collect$  to  $collect_{univ}$ 
4:   Sort and remove duplicates in  $collect_{univ}$ 
5: end procedure

```

by the auxiliary of $collect$, $g2u$ and $l2g_{next}$, as shown in Algorithm 6. We loop over rows of $l2g_{next}$ (i.e., elements in each process), and obtain each dof's $l2g_{next}$ value, which corresponds to the index of the $collect$ array. This $collect$ value further corresponds to the index of the finer level $g2u$ array. Using the hash_{g2u} , we finally compute the value in the $g2u_{next}$ array for this dof.

Algorithm 6 Compute $g2u_{next}$ map in next level

```

1:  $collect = \text{DOF\_NEXT}(l2g)$ 
2: procedure G2U_NEXT( $l2g_{next}, g2u$ )
3:   for  $e_i = 1 : \text{size}(l2g_{next}, 1)$  do
4:     for  $dof = 1 : \text{length}(l2g_{next}(e_i, :))$  do
5:        $coarse_{glb} = l2g_{next}(e_i, dof)$ 
6:        $fine_{glb} = collect(coarse_{glb})$ ;
7:        $fine_{univ} = g2u(fine_{glb})$ ;
8:        $g2u_{next}(coarse_{glb}) = \text{hash}_{g2u}(fine_{univ})$ ;
9:     end for
10:   end for
11: end procedure

```

2.4. Forming prolongation

With the help of $l2g$ and $g2u$ maps at each level, we are able to compute prolongation P as shown in Algorithm 7. We construct a sparse matrix in the COO format ² for P , denoted as P_{coo} .

²List of tuples of row, column, value.

We loop over elements in each process, and loop over each coarser level dof within this element. We find values in both coarser level $g2u_{next}$ map and finer level $g2u$ map for this dof, and set them to be the row and column indices in the universal system, respectively, and assign 1.0 (“injection” for modal basis ³) as the value in the COO structure. We append each COO structure of coarser level dofs in P_{COO} and remove duplicates.

Algorithm 7 Compute prolongation P

```

1: procedure COMP_PROL( $l2g, l2g_{next}, g2u, g2u_{next}$ )
2:   for  $e_i = 1 : \text{size}(l2g, 1)$  do
3:      $dc_{arr} = \text{EXTRACT\_NEXT\_DOF}(l2g(e_i, :))$ 
4:     for  $dof = 1 : \text{length}(dc_{arr})$  do
5:        $P_{col} = g2u_{next}(l2g_{next}(e_i, dof))$ 
6:        $P_{row} = g2u(dc_{arr}(dof))$ 
7:       Append  $(P_{row}, P_{col}, 1.0)$  to  $P_{coo}$ 
8:     end for
9:   end for
10:  Sort  $P_{coo}$  and remove duplicates
11: end procedure

```

2.5. *h*-coarsening

After reducing the basis order to the linear level, we employ the standard smoothed-aggregation AMG (SAAMG) approach to create coarser grids for h-coarsening. In this work, our previously developed open-source SAAMG library, Saena [25], is employed for this purpose. The aggregates and corresponding tentative prolongation are generated using a minimal independent set (MIS) approach. To smooth the tentative prolongation, an SPAI [33] smoother is employed. For more details about Saena, we refer readers to [25].

3. Experiments and results

In this section, we evaluate the performance of the GIAMG solver using the Helmholtz and the incompressible flow problems.

3.1. Helmholtz operator

We present a 3D Helmholtz operator posed on a unit cube domain with 8 elements using spectral/*hp* element. The equation is written as

$$-\nabla^2 u + \lambda u = f. \quad (2)$$

³GIAMG solver also has implementation for nodal basis, and it constructs prolongation matrix using interpolation instead of “injection”.

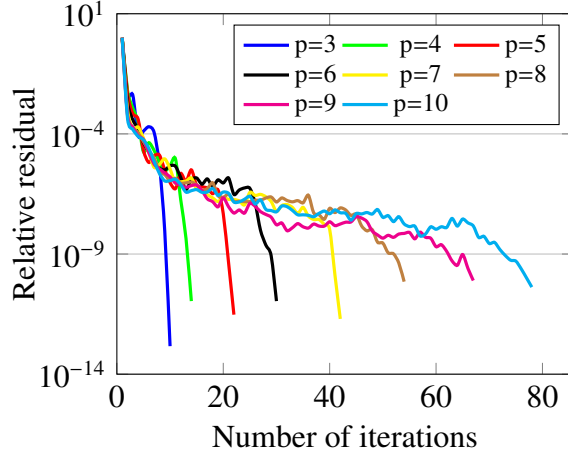


Figure 2: Convergence results of GIAMG from $p = 3$ to 10 for the Helmholtz operator.

In this case, we manufacture the forcing term f using an analytical solution as below

$$f = -(\lambda + 3\pi^2)\sin(\pi x)\sin(\pi y)\sin(\pi z) \quad (3)$$

$$u = \sin(\pi x)\sin(\pi y)\sin(\pi z) \quad (4)$$

λ is chosen to be 1.0 ⁴. Zero Dirichlet boundary condition is specified at all boundaries, and zero initial guess is employed. We only show the convergence results in this section, and we present detailed profiling and scaling results of the GIAMG approach in § 3.2.

3.1.1. Convergence results

We first plot the convergence for basis order from $p = 3$ to 10 using the GIAMG method by reducing the basis order by 2 at each level as shown in Figure 2. Note, in these cases, we only need to perform p -coarsening. We set the convergence criterion as the relative residual being less than 10^{-10} . We can see as we increase the basis order, the number of iterations does not significantly increase before a relative residual around 10^{-6} . The increase in the overall number of iterations is primarily because of the inability of the Chebyshev smoother to handle high-order discretizations, as has been shown in prior work [32].

3.1.2. Comparison with other solvers at $p = 8$

We compare the performance of the GIAMG method with other well-recognized multigrid packages, including PETSc GAMG, ML, and Hypre BoomerAMG solvers, at $p = 8$. Note, we call ML and BoomerAMG also via their PETSc interface. Since there are many components that affect the performance of multigrid solvers, and varied approaches have their own strategies and

⁴We note that the results do not extend to high-frequency Helmholtz problems.

	Smoother / Iterations	Coarsening scheme	Hierarchy Levels	Coarsest level size/nonzeros
GAMG	Chebyshev / 3	Default SA	4	21/441
ML	Chebyshev / 3	Uncoupled	4	23/365
BoomerAMG	Chebyshev / 3	HMIS	4	26/310
GIAMG	Chebyshev / 3	p -coarsening	4	27/343

Table 1: Key setup used in each multigrid approach at $p = 8$ for the Helmholtz operator.

parameters to handle different parts of multigrid, it is not possible to perform an exact comparison among different multigrid approaches. As a result, to initiate a reasonable comparison between all approaches, we keep some key parts in multigrid relatively comparable by tuning parameters in these parts for each approach according to our best knowledge. First of all, we use v-cycle for all cases. Secondly, note that in the coarsening part, GIAMG uses p -coarsening, while PETSc GAMG and ML use smoothed-aggregate method, and BoomerAMG uses the classical C-F splitting. The way we try to make the multigrid hierarchy fairly comparable is to ensure they all have the same number of levels and at the coarsest level, they have relatively comparable matrix sizes and numbers of nonzeros. Finally, we ensure that they all use the Chebyshev smoother during pre- and postsmothing with the same number of smoothing iterations. The breakdown of the key setup of different approaches is shown in Table 1. We also provide the performance of a diagonally preconditioned CG solver (DCG) implemented in *Nektar++* for comparison. Since the problem size is not too large, we can use a single core to test all the methods. The comparisons of the convergence and total solve time at $p = 8$ are plotted in Figure 3. We can see our GIAMG's convergence and

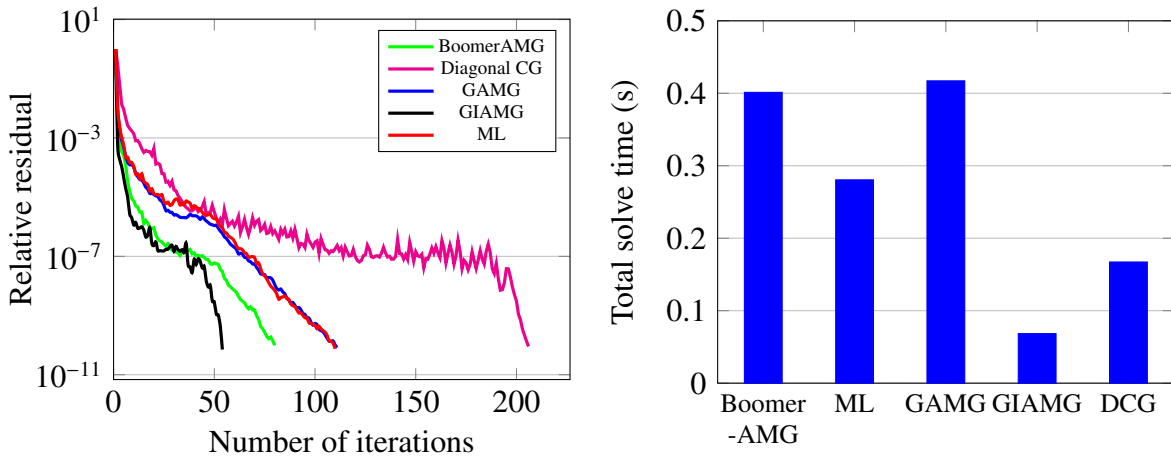


Figure 3: Convergence and solve time comparisons of GIAMG with PETSc GAMG, ML, BoomerAMG and DCG at $p = 8$ for the Helmholtz operator.

total solve time are both the best among all methods. Interestingly, in spite of DCG taking more iterations overall for convergence, it costs less solve time compared with other AMG approaches,

indicating AMG approaches (including GIAMG) take longer time to solve for one PCG iteration compared with DCG. GIAMG is the only AMG solver that is faster than DCG in terms of total solve time. Note that the overall solve time for GIAMG is significantly better than the other AMG solvers in part due to the fewer iterations it requires, but also because of the lower cost per iteration due to increased sparsity of the coarse-grid operators.

3.2. Incompressible flow problem

For the next evaluation, we solve for the 3D incompressible flow problem with a geometry based upon flow simulations with application to thermal transport in nuclear fusion modeling. The incompressible Navier–Stokes equations may be written as

$$\frac{\partial \mathbf{u}}{\partial t} + \mathbf{u} \cdot \nabla \mathbf{u} = -\nabla p + \nu \nabla^2 \mathbf{u} + \mathbf{f} \quad (5)$$

$$\nabla \cdot \mathbf{u} = 0 \quad (6)$$

where \mathbf{u} is the velocity, p is the pressure and ν is the kinematic viscosity. The governing equations are solved using a widely-adopted stiffly stable velocity correction scheme which splits the pressure and velocity fields. The velocity and pressure systems are decoupled resulting in four systems of rank N instead of a single coupled system of rank $4N$, where N denotes the total number of discretization points. The velocity correction scheme integrates the non-linear convection (i.e. first derivative) term explicitly in time whilst the pressure equation and diffusion (i.e. second derivative) term are integrated implicitly, requiring the solution of the Poisson and Helmholtz operators, respectively. Thus, the decoupled matrices are elliptic and symmetric. For detailed information on the velocity correction scheme implemented in *Nektar++*, we refer readers to [24, 34]. We note that solving the pressure field is typically the most challenging part in the velocity correction scheme, and therefore we focus on solving for pressure in the numerical experiments below.

The computational domain and mesh are shown in Figure 4, which represents a sample pin-type breeder blanket for a fusion reactor that is used in part to cool the reactor. In this application, a cooling fluid enters through the circular cross-section in the center of the pin, transports heat radiated at the opposite end of the pin and exits through the outer annulus. In this experiment, we do not consider the thermal transport terms, and focus on a under-resolved DNS at a Reynolds number of $Re = 10^4$ with a coarse mesh of 90,842 tetrahedra and 71,696 prisms, where the latter elements are used to resolve boundary layers in near-wall regions. The coarse nature of these simulations, together with large changes in velocity across a small region at the end of the pin, together with high aspect ratio elements at the walls, makes the systems particularly challenging to precondition at high order.

Boundary conditions are specified as a Poiseuille-type inflow condition supplied on the center

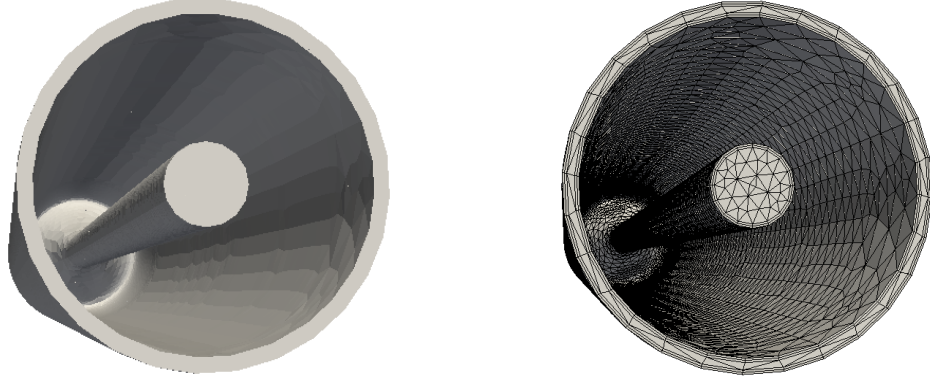


Figure 4: Geometry and mesh of the computational domain.

of the pin with a standard Neumann outflow condition supplied on the outflow (the outer annulus), and no-slip boundary conditions imposed on the remaining wall surfaces. Initial conditions to assemble the systems are the solutions after solving the governing equations for some time steps and reaching a physically-meaningful state. We only solve for one time step in our experiments since the matrices are not changing with time. Considering that very high order of basis function is typically not favored in practice for such a complex engineering application, we choose a reasonably high order of $p = 5$ as our maximum basis order in this example. The finest level matrix size and number of nonzeros are $6,604,956 \times 6,604,956$ and $1,129,952,608$, respectively. All the experiments (except the scaling experiment) are performed using 3 nodes with 40 cores on each node, resulting in a total 120 MPI tasks using University of Utah CHPC computing resources.

3.2.1. Convergence results

We plot the convergence results using GIAMG for p from 1 to 5 as shown in Figure 5. For this more complex system, we set the convergence criterion to be the relative residual less than 10^{-6} . In this case, we only reduce the basis order by 1 at each level during p -coarsening followed by 6 additional levels of coarsening using smoothed aggregation. We perform 2 Chebyshev iterations in pre- and postsmothing. The sizes and numbers of nonzeros of the coarsest level matrices in these cases are slightly different, varying from 303×303 to 315×315 , and 32338 to 34191, respectively, which are all reasonably small at the coarsest level for the superLU solver. We can see the number of iterations does not significantly increase as we increase p order. The convergence of $p = 3$ case looks slightly inferior to other cases. However, it still behaves within a reasonable range, and the convergence pattern is similar to that in other cases.

3.2.2. Detailed analysis at $p = 5$

We present a detailed analysis at $p = 5$ to comprehensively evaluate the performance of our GIAMG solver. All the timing presented in this section is the average across all processes. 6 levels

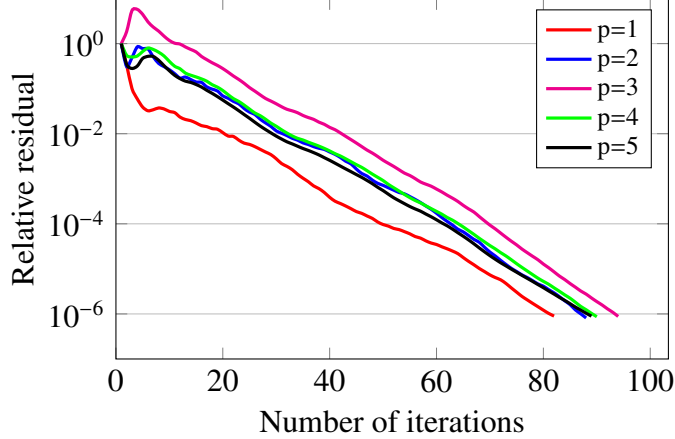


Figure 5: Convergence results for p from 1 to 5 for the incompressible flow problem.

of SA coarsening are used (as in the previous section) in all experiments except for the comparison with other multigrid packages, which is detailed in §3.2.2.5. The same machine is employed (as in the previous section to allow inter-order comparisons) except for the strong scaling experiments, which are presented in §3.2.2.4.

3.2.2.1 Breakdown profiling

We report breakdown profiling at $p = 5$ in Figure 6. We report the timings for different key parts of the v-cycle and the PCG solver. First, within the v-cycle, the pre- and postsmothing (2 smoothing iterations) dominate the total v-cycle time, with the smoothing at the first (finest) level being the most expensive of the total smoothing time. It is important to note that this will not be true if we do not employ p -coarsening, as the coarser levels will be denser and more expensive to evaluate. Intergrid transfer (residual restriction and error prolongation) only costs a small amount of time. Note, the superLU direct solver costs a negligible amount of time (indicating a small enough coarsest level system), and therefore it is not shown in Figure 6. In addition, the v-cycle preconditioning dominates the total time of PCG solver, which is mostly due to the matrix-vector multiplication in the pre- and postsmothing in v-cycle, and it makes the GIAMG much more expensive than a regular DCG solver for one PCG iteration. However, on the other hand, GIAMG has a much faster convergence. This motivates us to compare the total solve time of GIAMG with a regular DCG solver. We compare the GIAMG solver with the well-optimized DCG solver implemented in *Nektar++* for the solve time as shown in Figure 7. First of all, from Figure 6 (right) and Figure 7 (right), the time of matrix-vector multiplication looks similar in the two methods, which indicates it is a reasonable comparison between *Nektar++* and our GIAMG solver for the solve time even though they are two different implementations. Considering the dominant cost of v-cycle, our GIAMG is about 7 times as great as DCG in terms of the solve time in one PCG

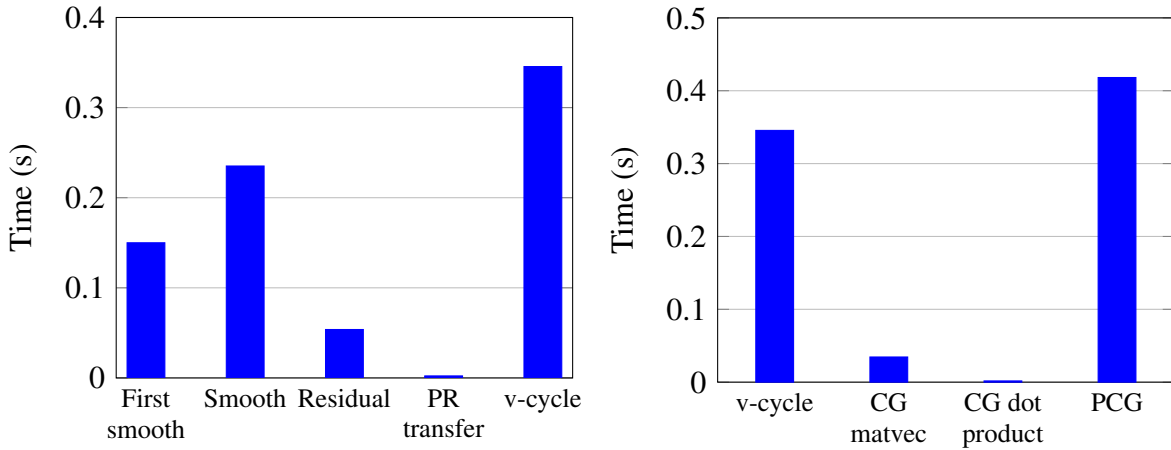


Figure 6: Breakdown profiling at $p = 5$ for the incompressible flow problem using GIAMG. (Left): profiling of v-cycle. “First smooth” refers to the Chebyshev smoothing time at the first level; “Smooth” refers to the time of Chebyshev smoothing at all levels; “Residual” refers to the time of computing residual, which is projected to the next coarser level; “PR transfer” refers to the time of residual restriction and error prolongation time; “v-cycle” refers to the total time of one v-cycle. (Right): profiling of PCG. “v-cycle” refers to the total time of one v-cycle; “CG matvec” refers to the time of the additional matrix-vector multiplication other than v-cycle in the PCG algorithm; “CG dot product” refers to the time of all additional dot product other than v-cycle in PCG; “PCG” refers to total time of one PCG iteration.

iteration. However, since DCG solver is about (3509 iterations) 40 times as great as our GIAMG solver in terms of the number of iterations for convergence, we are still about 6 times as fast as the DCG solver in terms of the overall solve time.

3.2.2.2 Number of Chebyshev smoothing iterations

Since smoothing time dominates the overall time of v-cycle, it is the most important part that we want to control for achieving overall solving efficiency. Less smoothing iterations will reduce the smoothing time, but on the other hand, it may not be able to provide a reasonable smoothing effect for a good convergence. This trade-off motivates us to perform the smoothing experiments as shown in Figure 8. We can see as increasing the number of smoothing iterations, the number of iterations for convergence generally decreases, while the time for smoothing as well as v-cycle increases. In addition, as we increase the number of smoothing iterations, the smoothing time becomes more and more dominant in the overall v-cycle time, further overshadowing other parts in the v-cycle. Specifically at $p = 5$, it can be concluded that the 2 smoothing iterations case is the optimal case in the experiments, and increasing number of smoothing iterations after it deteriorates overall solve performance, as the increased smoothing time overshadows the convergence gain. Note, the effect of smoothing may be varied for different basis orders and different problems.

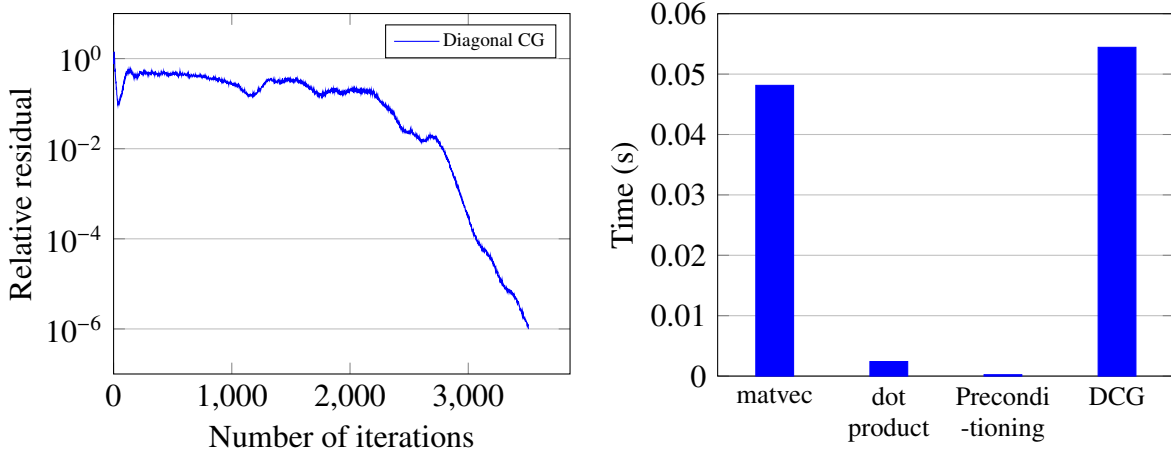


Figure 7: Breakdown profiling at $p = 5$ for the incompressible flow problem using DCG solver. (Left): convergence. (Right): profiling. "matvec" refers to the time of matrix-vector multiplication in the CG algorithm; "dot product" refers to the time of all dot product in the CG algorithm; "Preconditioning" refers to the time of applying diagonal preconditioner within DCG; "DCG" refers to total time of one DCG iteration.

3.2.2.3 *p*-coarsening strategy

Another key component that affects the GIAMG performance is the p -coarsening strategy. We test two coarsening strategies: (1), reducing basis order by 1 at each level (i.e., $5 \rightarrow 4 \rightarrow 3 \rightarrow 2 \rightarrow 1$); (2), reducing basis order by 2 at each level (i.e., $5 \rightarrow 3 \rightarrow 1$). The comparison is shown in Figure 9. The smoothing time is reduced when we coarsen the basis order by 2 at each level (the finest level smoothing time is still the same). The time saved here is essentially the second-finest level ($p = 4$) and the fourth-finest level ($p = 2$) compared with coarsening the basis order by 1. The residual computation time is also reduced as we have fewer levels to compute residuals when coarsening the basis order by 2. These result in a cheaper v-cycle for the more aggressive p -coarsening case. On the other hand, the number of iterations for convergence increases for the more aggressive p -coarsening, which is expected as it may introduce more aliasing error. However, the more aggressive p -coarsening case still achieves an overall better performance, indicating the time saved in the v-cycle overshadows the inferior convergence. Note again, the effect of p -coarsening strategies may also be order and problem specific.

3.2.2.4 Breakdown scalability

The strong scaling experiments are performed on the Frontera at the Texas Advanced Computing Center (TACC). The configuration of computing node used in the experiments is described below:

- Node:
 - Processor: Intel Xeon Platinum 8280 (“Cascade Lake”).

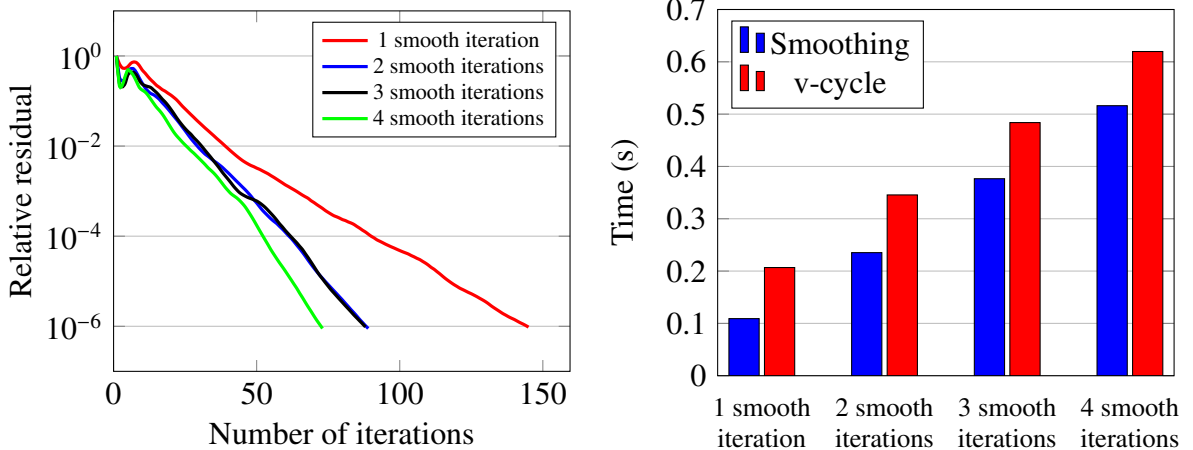


Figure 8: Comparison of different numbers of smoothing iterations at $p = 5$ for the incompressible flow problem. Note, we apply the same number of iterations in both pre- and postsmothing. (Left): convergence results. (Right) profiling of smoothing and v-cycle.

- Number of cores: 28 per socket, 56 per node.
- Clock rate: 2.7GHz (“Base Frequency”).
- “Peak” node performance: 4.8TF, double precision.
- Memory: *DDR* – 4 memory, 192GB/node.
- Network: Mellanox InfiniBand, HDR-100.

Figure 10 shows the strong scaling of v-cycle on 16 – 128 nodes. It can be concluded that our GIAMG method is able to be scaled up to 128 nodes (7168 MPI processes).

3.2.2.5 Comparison with other multigrid solvers

We present the comparisons of convergence and total solve time between GIAMG and other AMG solvers run from PETSc. Note, for this more complex system, making close comparisons is not as easy as for the Helmholtz operator in § 3.1.2. We try to make the overall comparisons as reasonable as possible according to our best knowledge of using these packages from PETSc. Some key parameters used in each AMG approach are shown in Table 2.

Our GIAMG method converges fastest among all the AMG packages under the relatively comparable conditions. In addition, it can be observed that other AMG solvers are stagnating at the relative residual around 0.1 at the beginning for about 200 iterations, while GIAMG does not suffer this stagnation during convergence. This can also be observed when using DCG solver but with a much longer stagnation time as shown in Figure 7 (left). We speculate it is the p -coarsening in GI-AMG that helps to achieve a significantly smoother convergence. After the stagnation period, all

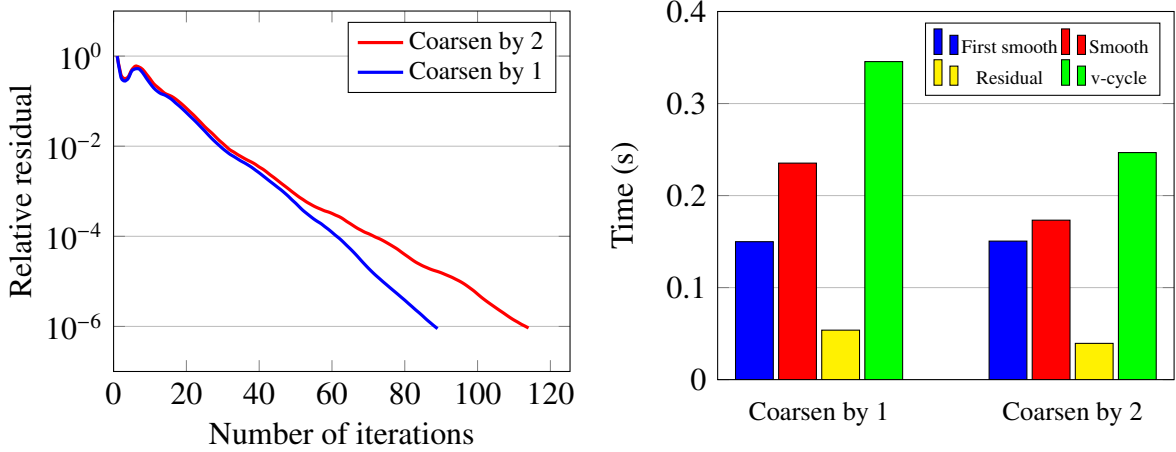


Figure 9: Comparison of different p -coarsening strategies at $p = 5$ for the incompressible flow problem. (Left): convergence results. (Right) profiling.

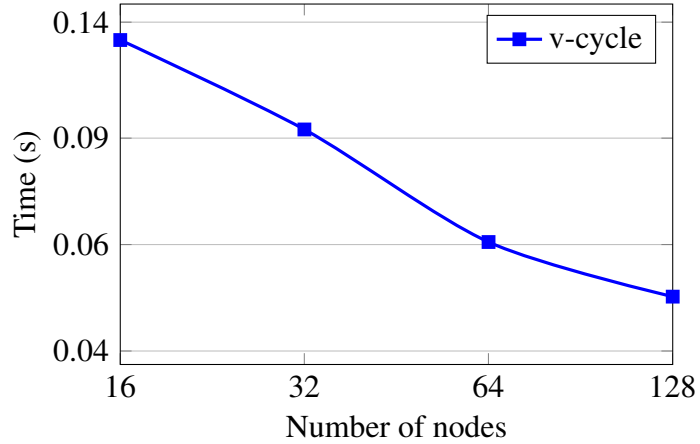


Figure 10: Strong scaling of v-cycle of GIAMG up to 128 nodes for the incompressible flow problem.

the AMG solvers seem to have a comparable convergence rate. The comparison of overall solve time is shown in Figure 11 (right). Again, our GIAMG solver performs the best among all the multigrid methods.

4. Conclusions and future work

In this paper, we proposed a geometrically informed algebraic multigrid (GIAMG) method, and developed an associated high-performance code for solving high-order finite element systems. The GIAMG method sets up a grid hierarchy that includes p -coarsening at the top grids with assistance of minimal information of the geometry from outside. We presented experiments for two 3D examples – Helmholtz and incompressible flow problem. For the Helmholtz operator, we showed the convergence results from $p = 3$ up to $p = 10$. The convergence rate does not significantly change as the p order is increasing. We also compared the convergence and solve

	Smoother / Iterations	Coarsening scheme	Hierarchy levels	Coarsest level size / nonzeros
GAMG	Chebyshev / 2	Default SA	6	240 / 57600
ML	Chebyshev / 2	MIS	6	736 / 35164
BoomerAMG	Chebyshev / 2	Falgout	7	602 / 51884
GIAMG	Chebyshev / 2	p -coarsening+SA	7	623 / 51072

Table 2: Some key parameters used in each multigrid approach at $p = 5$ for the incompressible flow problem.

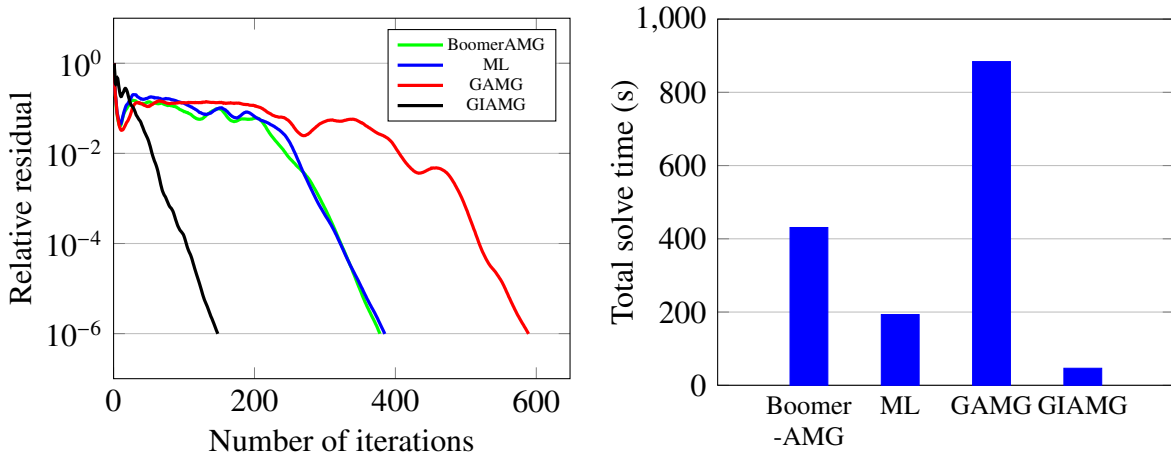


Figure 11: Comparison between multigrid methods at $p = 5$ for the incompressible flow problem. (Left): convergence result. (Right): total solve time

time with some well-recognized AMG packages and a standard diagonally preconditioned PCG solver implemented in *Nektar++*. Our GIAMG performed the best among all the solvers. For the incompressible flow problem, we presented the convergence results from $p = 1$ up to $p = 5$. The convergence is also order-independent as we increase p order. We further performed a detailed breakdown profiling of the GIAMG approach. The v-cycle dominates the PCG solving time, and pre- and postsmoothing take most time of the v-cycle. We are overall 6 times as fast as the diagonally preconditioned PCG solver. We further experimented on the effect of the number of smoothing iterations and p -coarsening strategies to the convergence and overall solve time. We also presented the strong scaling result of the GIAMG approach up to 128 nodes with 56 cores per node. Finally, we presented the comparisons of the GIAMG method with other AMG packages, and we again performed the best.

Our future work is to identify and extract the geometric information required at the finest level by the GIAMG method purely from input matrices, making GIAMG to be a complete AMG approach. We are currently able to identify local elements, or cliques, from input matrices. However, we are still working on how to correctly determine the dofs which should be restricted to next coarser level within each element, and form the prolongation operator based on this coarsening.

Acknowledgements

The authors greatly appreciate the computing resources provided by the University of Utah Center for High-Performance Computing (CHPC) and the NSF-funded University of Texas Austin Texas Advanced Computing Center (TACC) machine (use of Frontera). We additionally thank Dr. Andrew Davis and Dr. Aleksander Dubas (UK Atomic Energy Authority) for supplying the geometry used in § 3.2. MR acknowledges support from ARO W911NF-15-1-0222 (Program Manager Dr. Mike Coyle). DM acknowledges support from the EPSRC Platform Grant PRISM under grant EP/R029423/1 and the ELEMENT project under grant EP/V001345/1. SX, RMK and HS acknowledge that this research was partially sponsored by ARL under Cooperative Agreement Number W911NF-12-2-0023. The views and conclusions contained in this document are those of the authors and should not be interpreted as representing the official policies, either expressed or implied, of ARL or the U.S. government. The U.S. government is authorized to reproduce and distribute reprints for government purposes notwithstanding any copyright notation herein.

Appendix

In this section, we describe how *Nektar++* orders elemental dofs. For a hexahedron element type, *Nektar++* defines the modal basis at each dof using tensor products of 1D basis functions. 1D basis functions ϕ are defined recursively using Jacobi polynomial as Equation 7

$$\phi_p(a) = \begin{cases} \frac{1-a}{2} & \text{if } p = 0 \\ \frac{1+a}{2} & \text{if } p = 1 \\ \left(\frac{1-a}{2}\right)\left(\frac{1+a}{2}\right)P_{p-2}^{1,1}(a) & \text{otherwise,} \end{cases} \quad (7)$$

where p is the polynomial order, and a is the 1D coordinate. $P_p^{\alpha,\beta}$ is the p^{th} order Jacobi polynomial. For the linear case, we only have two modal basis functions in the element, $\frac{1-a}{2}$ and $\frac{1+a}{2}$, called the “vertex modes”, which coincides with the case of linear nodal basis. For high-order cases, higher order polynomials, the so-called “edge modes” and “interior modes”, are introduced. The 3D basis Φ for an order p hexahedron element at each dof is defined as a tensor product of 1D basis functions

$$\Phi_{(p+1)^2 \times i+(p+1) \times j+k} = \phi_i \times \phi_j \times \phi_k \quad (8)$$

Equation 8 also determines the ordering of the $(p+1) \times (p+1) \times (p+1)$ dofs within the hexahedron element in *Nektar++*, i.e., the $((p+1)^2 \times i + (p+1) \times j + k)^{\text{th}}$ basis function is associated to the $((p+1)^2 \times i + (p+1) \times j + k)^{\text{th}}$ dof in the elemental dof collection, implying that the order of this dof is i, j , and k in the x, y and z directions of the coordinate system, respectively. For

the spectral/ hp element basis definitions of other element types, we refer readers to [2] for more detailed information.

References

- [1] D. A. Kopriva. *Implementing spectral methods for partial differential equations: Algorithms for scientists and engineers*. Springer Science & Business Media, 2009.
- [2] G. Karniadakis and S. Sherwin. *Spectral/hp Element Methods for Computational Fluid Dynamics: Second Edition*. Numerical Mathematics and Scientific Computation. OUP Oxford, 2013.
- [3] A. N. Brooks and T. J.R. Hughes. Streamline upwind/Petrov-Galerkin formulations for convection dominated flows with particular emphasis on the incompressible Navier-Stokes equations. *Computer Methods in Applied Mechanics and Engineering*, 32(1-3):199–259, 1982.
- [4] F. Bassi and S. Rebay. A high-order accurate discontinuous finite element method for the numerical solution of the compressible navier–stokes equations. *Journal of Computational Physics*, 131(2):267–279, 1997.
- [5] G. E. Karniadakis, M. Israeli, and S. A. Orszag. High-order splitting methods for the incompressible Navier-Stokes equations. *Journal of Computational Physics*, 97(2):414–443, 1991.
- [6] H. T. Huynh, Z. H. Wang, and P. E. Vincent. High-order methods for computational fluid dynamics: A brief review of compact differential formulations on unstructured grids. *Computers & Fluids*, 98:209–220, 2014.
- [7] J.-E. W. Lombard, D. Moxey, S. J. Sherwin, J. F. A. Hoessler, S. Dhandapani, and M. J. Taylor. Implicit large-eddy simulation of a wingtip vortex. *AIAA Journal*, 54(2):506–518, 2016.
- [8] G. Mengaldo, D. Moxey, M. Turner, R. C. Moura, A. Jassim, M. Taylor, J. Peiró, and S. J. Sherwin. Industry-relevant implicit large-eddy simulation of a high-performance road car via spectral/ hp element methods. *SIAM Review*, (4):723–755, 2021. doi: 10.1137/20M1345359. URL <https://arxiv.org/pdf/2009.10178.pdf>.
- [9] N. Fehn, W. A. Wall, and M. Kronbichler. Robust and efficient discontinuous Galerkin methods for under-resolved turbulent incompressible flows. *Journal of Computational Physics*, 372:667–693, 2018.

- [10] D. Moxey, R. Amici, and R. M. Kirby. Efficient matrix-free high-order finite element evaluation for simplicial elements. *SIAM Journal on Scientific Computing*, 42:C97–C123, 2020.
- [11] U. Trottenberg, C. W. Oosterlee, and A. Schuller. *Multigrid*. Elsevier, 2000.
- [12] K. J. Fidkowski, T. A. Oliver, J. Lu, and D. L. Darmofal. p-multigrid solution of high-order discontinuous galerkin discretizations of the compressible navier–stokes equations. *Journal of Computational Physics*, 207(1):92–113, 2005.
- [13] B. T. Helenbrook and H. L. Atkins. Application of p-multigrid to discontinuous galerkin formulations of the poisson equation. *AIAA journal*, 44(3):566–575, 2006.
- [14] B. Helenbrook, D. Mavriplis, and H. Atkins. Analysis of “p”-multigrid for continuous and discontinuous finite element discretizations. In *16th AIAA Computational Fluid Dynamics Conference*, page 3989, 2003.
- [15] I. Huismann, J. Stiller, and J. Fröhlich. Scaling to the stars—a linearly scaling elliptic solver for p-multigrid. *Journal of Computational Physics*, 398:108868, 2019.
- [16] D. A. May, J. Brown, and L. Le Pourhiet. A scalable, matrix-free multigrid preconditioner for finite element discretizations of heterogeneous stokes flow. *Computer methods in applied mechanics and engineering*, 290:496–523, 2015.
- [17] J. Brown. Efficient nonlinear solvers for nodal high-order finite elements in 3d. *Journal of Scientific Computing*, 45(1-3):48–63, 2010.
- [18] S. D. Kim. Piecewise bilinear preconditioning of high-order finite element methods. *Electronic Transactions on Numerical Analysis*, 26:228–242, 2007.
- [19] L. Olson. Algebraic multigrid preconditioning of high-order spectral elements for elliptic problems on a simplicial mesh. *SIAM Journal on Scientific Computing*, 29(5):2189–2209, 2007.
- [20] M. O. Deville and E. H. Mund. Finite-element preconditioning for pseudospectral solutions of elliptic problems. *SIAM Journal on Scientific and Statistical Computing*, 11(2):311–342, 1990.
- [21] C. Canuto, P. Gervasio, and A. Quarteroni. Finite-element preconditioning of g-ni spectral methods. *SIAM Journal on Scientific Computing*, 31(6):4422–4451, 2010.
- [22] J. J. Heys, T. A. Manteuffel, S. F. McCormick, and L. N. Olson. Algebraic multigrid for higher-order finite elements. *Journal of computational Physics*, 204(2):520–532, 2005.

- [23] C. D. Cantwell, D. Moxey, A. Comerford, A. Bolis, G. Rocco, G. Mengaldo, D. De Grazia, S. Yakovlev, J. E. Lombard, D. Ekelschot, B. Jordi, H. Xu, Y. Mohamied, C. Eskilsson, B. Nelson, P. Vos, C. Biotto, R. M. Kirby, and S. J. Sherwin. Nektar++: An open-source spectral/hp element framework. *Computer Physics Communications*, 192:205–219, 2015.
- [24] D. Moxey, C. D. Cantwell, Y. Bao, A. Cassinelli, G. Castiglioni, S. Chun, E. Juda, E. Kazemi, K. Lackhove, J. Marcon, G. Mengaldo, D. Serson, M. Turner, H. Xu, J. Peiró, R. M. Kirby, and S. J. Sherwin. Nektar++: Enhancing the capability and application of high-fidelity spectral/hp element methods. *Computer Physics Communications*, 249:107110, 2020.
- [25] M. Rasouli, V. Zala, R. M. Kirby, and H. Sundar. Improving performance and scalability of algebraic multigrid through a specialized matvec. In *2018 IEEE High Performance extreme Computing Conference (HPEC)*, pages 1–7, 2018.
- [26] W. Bangerth, R. Hartmann, and G. Kanschat. deal. ii—a general-purpose object-oriented finite element library. *ACM Transactions on Mathematical Software (TOMS)*, 33(4):24–es, 2007.
- [27] A. D. Lindsay, D. R. Gaston, C. J. Permann, J. M. Miller, D. Andrš, A. E. Slaughter, F. Kong, J. Hansel, R. W. Carlsen, C. Icenhour, L. Harbour, G. L. Giudicelli, R. H. Stogner, P. German, J. Badger, S. Biswas, L. Chapuis, C. Green, J. Hales, T. Hu, W. Jiang, Y. S. Jung, C. Matthews, Y. Miao, A. Novak, J. W. Peterson, Z. M. Prince, A. Rovinelli, S. Schunert, D. Schwen, B. W. Spencer, S. Veeraraghavan, A. Recuero, D. Yushu, Y. Wang, A. Wilkins, and C. Wong. 2.0 - MOOSE: Enabling massively parallel multiphysics simulation. *SoftwareX*, 20:101202, 2022.
- [28] R. Anderson, J. Andrej, A. Barker, J. Bramwell, J.-S. Camier, J. Cerveny V. Dobrev, Y. Du-douit, A. Fisher, Tz. Kolev, W. Pazner, M. Stowell, V. Tomov, I. Akkerman, J. Dahm, D. Medina, and S. Zampini. MFEM: A modular finite element methods library. *Computers & Mathematics with Applications*, 81:42–74, 2021.
- [29] M. W. Gee, C. M. Siefert, J. J. Hu, R. S. Tuminaro, and M. G. Sala. MI 5.0 smoothed aggregation user’s guide. Technical report, Citeseer, 2006.
- [30] R. D. Falgout and U. M. Yang. hypre: A library of high performance preconditioners. In *International Conference on Computational Science*, pages 632–641. Springer, 2002.
- [31] X. S. Li. An overview of superlu: Algorithms, implementation, and user interface. *ACM Transactions on Mathematical Software (TOMS)*, 31(3):302–325, 2005.

- [32] H. Sundar, G. Stadler, and G. Biros. Comparison of multigrid algorithms for high-order continuous finite element discretizations. *Numerical Linear Algebra with Applications*, 22(4):664–680, 2015.
- [33] O. Bröker and M. J. Grote. Sparse approximate inverse smoothers for geometric and algebraic multigrid. *Applied numerical mathematics*, 41(1):61–80, 2002.
- [34] G. E. Karniadakis, M. Israeli, and S. A. Orszag. High-order splitting methods for the incompressible navier-stokes equations. *Journal of Computational Physics*, 97(2):414 – 443, 1991.